Master's Thesis

Title

Proposal and Evaluation of Robot Navigation Methods Utilizing Radio Wave Simulators in a Private 5G Environment

Supervisor

Associate Professor Shin'ichi Arakawa

Author

YU YANG

February 3rd, 2025

Department of Information Networking

Graduate School of Information Science and Technology

Osaka University

Master's Thesis

Proposal and Evaluation of Robot Navigation Methods Utilizing Radio Wave Simulators in a Private 5G Environment

YU YANG

Abstract

In recent years, the advancement of wireless communication technologies has pointed 5G as a pivotal element in achieving high - reliability and low-latency communication systems. Compared to its predecessor, LTE (Long Term Evolution), 5G offers significant improvements in data transmission rates, latency, network capacity, and spectral efficiency. Specifically, 5G can achieve peak download speeds up to 20 Gbps, a substantial increase from LTE's theoretical maximum of approximately 1 Gbps. Additionally, 5G boasts ultra-low latency of around 1 millisecond, compared to LTE's 30-50 milliseconds, which is crucial for real-time applications such as autonomous driving and remote surgery.

However, the use of higher frequency bands deployed in 5G, such as millimeter waves, results in limited coverage areas and reduced penetration through obstacles, necessitating a denser network of base stations . Among the various applications of 5G, autonomous robots stand out due to their reliance on reliable and continuous network connectivity for effective operation. In domains such as warehousing, logistics, patrolling, and guided navigation, the enhanced capabilities of 5G facilitate improved efficiency and safety. For instance, 5G-enabled Automated Guided Vehicles (AGVs) can perform more precise scheduling and routing, while drones connected via 5G networks can conduct safer inspections and remote monitoring tasks.

Neverthless, the widespread deployment of autonomous robots faces a sustainability challenge: ensuring reliable communication to maintain the continuous network connections necessary for task execution. In urban environments, wireless signals are susceptible to multipath fading, obstacles, and environmental changes, leading to dynamic fluctuations in received signal strength (RSS), there is still room for improvement in achieving

precise predictions. Due to resource constraints, large-scale RSS sampling is costly, making it challenging for robots to plan navigation paths that ensure communication continuity while efficiently reaching their destinations. Furthermore, 5G high-frequency bands are more susceptible to multipath effects compared to LTE due to their shorter wavelengths, higher directionality, and greater sensitivity to environmental changes . Multipath effects can cause rapid signal fluctuations, thereby affecting data transmission and even leading to network disconnections. This necessitates more sophisticated signal processing and navigation strategies in 5G high-frequency band communications. This study addresses these issues by developing a navigation strategy that fully utilizes sensors, including cameras, to acquire physical environmental information in 5G environments, thereby enhancing the accuracy of signal strength prediction. This enables robots to maintain reliable communication links while moving from a start point to a destination. The strategy involves predicting the spatial distribution of Reference Signal Received Power (RSRP) based on the information of the traversed space, even with minimal prior data, and designing an method that integrates RSRP into the navigation process. The importance of this method lies in its ability to prevent severe mission-critical issues that may arise from communication interruptions, particularly in applications requiring data exchange or coordination. Therefore, the method designed in this study improves the operational reliability of robots by enhancing RSRP prediction and incorporating signal factors into navigation decision-making.

Keywords

Fifth-Generation (5G) Wireless Communication

Robot navigation

Reference Signal Received Power (RSRP) prediction

Multipath fading

Gaussian process regression(GPR)

Signal propagation modeling

Contents

List of Figures

List of Tables

1 Introduction

In recent years, advancements in wireless communication technologies have pointed 5G as a pivotal element in achieving high-reliability and low-latency communication systems. Compared to its predecessor, LTE (Long Term Evolution), 5G offers significant improvements in data transmission rates, latency, network capacity, and spectral efficiency [1]. Specifically, 5G can achieve peak download speeds of up to 20 Gbps, a substantial increase from LTE's theoretical maximum of approximately 1 Gbps. Additionally, 5G boasts ultra-low latency of around 1 millisecond, compared to LTE's between 30 to 50 milliseconds, which is crucial for real-time applications such as autonomous driving and remote surgery.

However, the deployment of 5G presents several challenges. The use of higher frequency bands, such as millimeter waves, results in limited coverage areas and reduced penetration through obstacles, necessitating a denser network of base stations [2]. Among the various applications of 5G, autonomous robots stand out due to their reliance on continuous and reliable network connectivity for effective operation. In domains such as warehousing, logistics, patrolling, and guided navigation, the enhanced capabilities of 5G facilitate improved efficiency and safety. For instance, 5G-enabled Automated Guided Vehicles (AGVs) can perform more precise scheduling and routing, while drones connected via 5G networks can conduct safer inspections and remote monitoring tasks.

Despite these advantages, ensuring reliable communication for autonomous robots remains a critical challenge. In urban environments, radio signals are susceptible to multipath fading, obstacles, and environmental variations, leading to dynamic fluctuations in received signal strength (RSS). Precise prediction of these variations remains challenging. Large-scale sampling is costly and impractical, making it difficult for robots to plan navigation paths that guarantee communication continuity while optimizing travel efficiency. Furthermore, the higher-frequency bands used in 5G are more susceptible to multipath effects compared to LTE due to their shorter wavelengths, higher directionality, and greater sensitivity to environmental changes [3]. These multipath effects can cause rapid signal fluctuations, affecting data transmission and even leading to network disconnections. Consequently, more sophisticated signal processing and navigation strategies are required to maintain connectivity in 5G high-frequency band communications.

Maintaining network connectivity is crucial for mission-critical tasks that involve information collection and real-time data transmission. For example, in remote monitoring or operations conducted in urban environments, even with relatively reliable 2D maps, robots may still experience network disconnections during execution. Predicting network connectivity is highly complex since signals attenuate with distance from the transmitter (Tx) and are further affected when obstacles obstruct the propagation path between the receiver (Rx) and Tx. When combined with complex fading phenomena, such as multipath fading, these factors can create isolated no-connection zones [4]. To avoid such regions, human operators or autonomous decision-making systems must proactively estimate connectivity conditions along the planned path.

To address this issue, it is essential to provide robots with a stable and reliable network connection during operation. Our method ensures network connectivity by predicting RSRP values and disconnection probabilities as the Signal coefficient factor , and incorporating this Signal coefficient factor into the navigation method. In this paper, we propose a navigation method that integrates both Distance Cost and Signal coefficient factor while utilizing Building Information Model (BIM). It consists of three key components: First, we utilize BIM and ray-tracing-based radio simulation software to estimate the RSRP distribution in the environment. Second, we employ a spatial prediction model based on GPR to dynamically update the RSRP distribution. Third, we predict the probability of disconnection in unexplored areas using a spatial Bayesian method that estimates the Nakagami-m distribution based on RSRP sampled data. This probability is then integrated into the navigation method along with distance and RSRP information. The remainder of this paper is organized as follows. Section 2 reviews existing studies on the reliable network connection navigation problem. Section 3 formulates the problem statement, outlining the specific challenges we aim to tackle. Section 4 presents the implementation details of our proposed method. Section 5 describes the experimental setup and discusses the results obtained. Finally, Section 6 summarizes the findings and concludes the paper.

2 Related Work

Significant efforts have been made to address the issue that maintain robust wireless communication between mobile robots and base stations[5] [6] .Some researchers have focused on Communication-Aware Motion (or Path) Planning (CAMP), which simultaneously optimizes movement and communication constraints to find and execute the optimal path to the destination [7] .Others proves that reliable wireless connectivity is vital for mobile robot control and data communication

[8].[9]

Yan et al. use an intelligent AUV system integrates binocular cameras, sonars, and acoustic modems for obstacle avoidance and communication. A depth deterministic policy gradient (DDPG) method optimizes motion planning by balancing communication quality and stability, outperforming disk-model and distance-based methods. Simulations and experiments validate its effectiveness in complex underwater environments. [10] However, this method still lacks adaptability to dynamic environments.

The Kalman filter method has also been used for rapid prediction of signal strength along paths. Compared to methods like Gaussian process regression, the Kalman filter makes fewer assumptions about the environment, offering better adaptability in dynamic scenarios and higher computational efficiency [11]. Nevertheless, the Kalman filter can only predict the signal strength at the next point, unabling to assess wireless connectivity quality across the environment. The aforementioned prediction studies address small-scale fading by modeling it with longer time windows, such as applying Spatial Moving Average Filters to average RSS observation data. Even so, they overlook the rapid fluctuations of small-scale fading within short time frames, which may lead to brief disconnections—undesirable conditions.

However, in [12], the RSS prediction is solely based on the observed RSS data and does not effectively leverage the geometric information inherent in the environment. This limitation prevents the method from fully exploiting all available spatial cues that could further enhance signal prediction accuracy and robustness.

Apart from the aforementioned issues,navigation is also an essential task in the field of mobile robotics.When a robot performs navigation tasks that require maintaining net-

work connection under the circumstance of global navigation, the prior knowledge of the environment should be available.[13] However, in practical situations ,it is challenging to obtain all radio information within the map in advance. And in the local navigation, though the robot can decide or control its motion and orientation autonomously using equipped sensors [13],radio wave propagation is closely related to the geometric information of the environment, and relying solely on observed data for prediction has certain limitations. Hence,it is becoming increasingly important to achieve network connection navigation with minimal prior information and more accurate model. In our paper, we refer to the problem of planning a path that both minimizes the travel distance and minimizes the risk of communication interruption. Although in some references this problem is referred to as the "communication-aware path planning problem", we have chosen to use the term "reliable network connection navigation" problem throughout this paper for consistency. For the remainder of this paper, we adopt the unified terminology of the reliable network connection navigation problem. This decision is made to maintain consistency in our discussion and avoid potential confusion. Overall,It can be seen that maintaining a stable signal connection while achieving accurate real-time route planning in complex environments is a challenging problem. Therefore, the purpose of this study is to propose a method that considers not only Signal coefficient factor but also Distance Cost in navigation using mall-area private 5G systems, a.k.a, Local 5G systems in Japan. Signal coefficient factor of static signal value is predicted by using 3D model, and signal uncertainty is calculated by using spatial Bayesian method and empirical model (Nakagami-m distribution). In order to achieve reliable network connection navigation with minimal prior information, the following methods are considered: using detailed parameters of Local 5G access point (AP) locations and incorporating geometric information from an imprecise BIM as input, which includes shape and material information. we will use the the available BIM and ray-tracing simulation to estimate the RSRP by simulating signal reflection and refraction based on buildings and obstacles in the BIM. Ray-tracing simulation does not consider signal fluctuation caused by dynamic obstacles, which may cause the robot to network disconnection. To avoid the network disconnection cause by signal fluctuation , we calculate the probability that the RSRP falls below the threshold that leads to a disconnect, we use a spatial Bayesian method to estimate the necessary

parameters of disconnect calculation. In our method, we estimate the Nakagami-m distribution parameters that characterize the shape and average power of the sampled data by incorporating both the observed RSRP data and the spatial context provided by the environment. Once these parameters are estimated, these parameters are used to compute the likelihood that RSRP will drop below the disconnect threshold, thus quantifying the probability of disconnection at a given location. Finally, we combine RSRP, the probability of disconnection, and the Distance Cost to target point to design a navigation method that maintains reliable network connectivity.

3 Problem Formulation for Reliable Network Connection Navigation in 5G-Enabled Autonomous Robots

3.1 Problem Background

In our research context, the robot is deployed to perform monitoring and data collection tasks in a 5G environment with the primary target of ensuring reliable network connectivity throughout the mission. The start point S and the target point T are set by the task planner according to the specific application (e.g., delivery, inspection, etc.).

The start point S and target point T are typically predetermined by the task planner or operator based on the mission requirements. For example, in inspection or delivery tasks, the task planner selects appropriate start and target points to ensure that the robot can successfully complete the mission. In this work, the autonomous navigation robot is deployed in a 5G network environment, and its main tasks include real-time data collection, environmental monitoring, and remote control. To accomplish these tasks, the robot must maintain a stable network connection throughout its navigation so that it can receive remote commands and transmit collected data.

The robot is required to navigate from the start point S to the target point T in a two-dimensional workspace. In the path calculation, it is necessary not only to minimize the Distance Cost but also to account for the risk of network disconnection so that the signal strength requirements are satisfied along the entire path. After reaching the target point T, the robot will perform subsequent tasks such as data collection, on-site inspection, or environmental monitoring. Therefore, maintaining high-quality network connection during navigation is essential for mission success. Although the robot is capable of autonomous navigation, tasks such as real-time data transmission, remote monitoring, and multi-robot collaboration in a 5G environment require the system to maintain a stable network connection at all times. Thus, in navigation, both the minimization of the Distance Cost and the reduction of the risk ofnetwork disconnection must be considered to ensure mission continuity and safety.

3.2 Environmental Assumptions

3.2.1 Workspace Definition

The robot operates in a two-dimensional plane embedded in a three-dimensional space that contains static obstacles, denoted by $\mathcal{O}$. In this environment, static obstacles are present, and initially the system is provided with partial prior information regarding the approximate points and outer contours of these obstacles, as well as the coordinates of the AP. However, details such as the precise material properties and the heights of the obstacles are not known. We will use the RSRP, which offers a more robust and consistent measure of channel conditions, as the indicator of signal strength.

3.2.2 Robot Kinematic Constraints

To ensure the stability and safety of the robot during motion, its speed must be constrained. The specified maximum speed, $V_{\max}$, reflects both the physical capabilities of the robot platform and the mission's safety requirements. Regarding turning angles, we assume that the robot can stop and perform an in-place rotation when changing its heading; therefore, no constraint is imposed on the turning angle in our study. We assume that the path traversed by the robot during the mission is given by

$$P = [S = (x_0, y_0), (x_1, y_1), (x_2, y_2), \ldots, (x_{N-1}, y_{N-1}), (x_N, y_N) = T],$$

which comprises a start point S, a target point T, and $N - 2$ intermediate points. For any point along the path, we denote its coordinates as (x_i, y_i) for $i = 0, 1, \ldots, N$, and the velocity vector at point (x_i, y_i) is denoted by $\mathbf{v}_{(x_i, y_i)}$. Note that N is not a constant value but it varies dependent on the path planning. To ensure mission safety and equipment integrity, the robot must avoid obstacles; that is, none of the points along the path may lie within an obstacle.

In summary, the robot motion is constrained by:

$$\|\mathbf{v}_{(x_i, y_i)}\| \leq V_{\max} \qquad \text{(Maximum velocity)},$$

$$(x_i, y_i) \notin \mathcal{O} \qquad \forall\, (x_i, y_i) \in P \quad \text{(Obstacle avoidance)}.$$
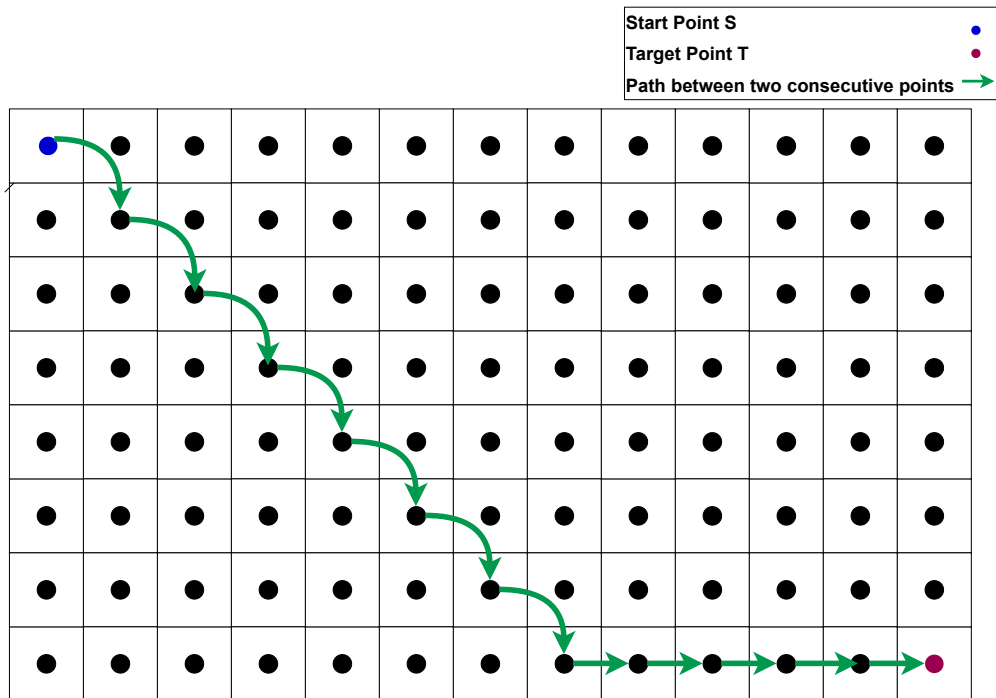
Figure 1: In a 2D grid map, the start point S, target point T, and the path between two consecutive points are shown. Blue dot: start point S; red dot: target point T; green arrow: path between two consecutive points.

3.3 Optimization Problem

3.3.1 Decision Variables

A path consists of a sequence of consecutive segments. By summing the lengths of all the segments, the total length of the path can be determined. We assume that the path

$$P = [S = (x_0, y_0), (x_1, y_1), (x_2, y_2), \ldots, (x_{N-1}, y_{N-1}), (x_N, y_N) = T]$$

comprises a start point S, a target point T, and n intermediate points, as illustrated in Fig. 1. Here, n represents the number of intermediate or rotation points (RPs). Thus, a segment of the path is formed by two consecutive points.

3.3.2 Objective Function

The safety and efficiency of the robot during its mission are quantified by a cost function $c(P)$, where $P = [S = (x_0, y_0), (x_1, y_1), (x_2, y_2), \ldots, (x_{N-1}, y_{N-1}), (x_N, y_N) = T]$ represents the sequence of path points traversed by the robot during the mission. Specifically, the mission cost is divided into two components: Distance Cost and Signal coefficient factor . The Euclidean distance between two consecutive points, $\|(x_{i+1}, y_{i+1}) - (x_i, y_i)\|$, represents the estimated distance from (x_i, y_i) to (x_{i+1}, y_{i+1}), where (x_i, y_i) and (x_{i+1}, y_{i+1}) represent two consecutive points of the path P. The Signal coefficient factor for moving from point (x_i, y_i) to the next point (x_{i+1}, y_{i+1}) is characterized by the average measured RSRP $\overline{rsrp_{(x_{i+1}, y_{i+1})}}$, and the probability of network disconnection at that point, $\rho(x_{i+1}, y_{i+1})$. For each segment, both the Distance Cost and the Signal coefficient factor are considered, and the total cost $c(P)$ is obtained by summing the costs between all consecutive points along the path. Here, λ_1 and λ_2 are the weighting coefficients for $\overline{rsrp_{(x_{i+1}, y_{i+1})}}$ and $\rho(x_{i+1}, y_{i+1})$, respectively, which balance their influence on the navigation in different scenarios. The objective is to minimize the hybrid cost $c(P)$ that combines both the Distance Cost and the Signal coefficient factor :

$$\min_P c(P) = \sum_{i=0}^{N-1} \underbrace{\|(x_{i+1}, y_{i+1}) - (x_i, y_i)\|}_{\text{Distance Cost}} \cdot \underbrace{\left(\lambda_1 \overline{rsrp_{(x_{i+1}, y_{i+1})}} + \lambda_2 \rho(x_{i+1}, y_{i+1}) \right)}_{\text{Signal coefficient factor}}. \quad (1)$$

3.4 Complete Problem Statement

In this paper, we model the autonomous navigation task as an optimization problem. To ensure reliable data transmission during the mission, the average measured RSRP at every point $(x_i, y_i) \in P$ along the path must satisfy

$$\overline{rsrp_{(x_i, y_i)}} \geq -120 \, \text{dBm}.$$

At the same time, to maintain network connectivity throughout the mission, the probability of network disconnection $\rho(x_i, y_i)$ at each point should be as low as possible, while the Distance Cost is minimized under good signal conditions. The objective function integrates both the Distance Cost and the risk of network disconnectiom. The reliable network

connection navigation problem is formally expressed as:

$$\min_{P} \quad c(P) = \sum_{i=0}^{N-1} \|(x_{i+1}, y_{i+1}) - (x_i, y_i)\| \left(\lambda_1 \overline{rsrp_{(x_{i+1}, y_{i+1})}} + \lambda_2 \rho(x_{i+1}, y_{i+1})\right),$$

$$\text{Subject to} \quad (x_i, y_i) \notin \mathcal{O}, \quad \forall\, (x_i, y_i) \in P,$$

$$\|\mathbf{v}_{(x_i, y_i)}\| \leq V_{\max}, \quad \forall\, (x_i, y_i) \in P.$$

4 Signal coefficient factor Prediction and Distance-Based Integration Navigation Method

4.1 System Overview

The proposed system is comprised of three core components that work together to achieve reliable signal connected navigation with minimal prior information. First, the ray-tracing simulation leverages BIM to generate estimates of the RSRP across the environment. This RSRP serves as the foundation for further refinement.

Secondly, the prediction module employs GPR to continuously update the RSRP in the environment based on real-time measurements, enabling the system to adapt to dynamic changes in the signal environment. At the same time, we use the observed RSRP data and a spatial Bayesian method to predict the disconnection probability within the environment. Finally, the navigation module integrates the predicted RSRP, the predicted disconnection probability, and the Distance Cost to plan a path that maintains stable signal connectivity. Our method is designed to enable robots to navigate autonomously in radio environments that are either unknown or only partially known, while ensuring that the signal strength meets threshold requirements. Initially, the robot obtains preliminary estimates of the signal strength through ray-tracing simulations and employs Gaussian Process Regression (GPR) to update the channel state in real time. After each movement, The robot measures the signal strength at its current location and calculates the Signal coefficient factor for reaching the next point based on both the predicted rsrp and the disconnection probability. Subsequently, the robot replans the optimal path from its current point to the target, selecting a route that not only minimizes the travel distance but also mitigates the risk of signal disconnection.

When the signal strength along the new path falls below the preset threshold, the robot does not proceed further. Instead, it backtracks to the most recent location where the RSRP was still acceptable and recalculates the path, thereby ensuring network connectivity throughout the navigation process.

This method enables the robot to dynamically adapt to changes in the signal environment while minimizing the overall path cost. Even without detailed radio maps at the

outset, the robot can progressively learn and optimize its path as it navigates.

The pseudocode in 1 also describes the process of the navigation method. Here, $(x_c, y_c), c = 0, 1 \ldots, N$ represents the current point on the path P, P denotes the path from the start point to the current point, and $\overline{rsrp_{(x_c,y_c)}}$ represents the measured average RSRP at point (x_c, y_c).

Then, we compute the cost of reaching the next point using the cost function $c(P)$. If the RSRP at the next point is above the threshold $\tau = -140\,\text{dBm}$, the robot proceeds to that point; otherwise, it backtracks to the most recent safe point.

Algorithm 1 Integration of Signal coefficient factor and Distance Cost in Navigation

---

1: Initialize Path $P \leftarrow [(x_0, y_0) = S]$

2: Update M_{rsrp} using ray-tracing simulation and BIM

3: **while** $(x_c, y_c) \neq T$ **do**

4:     Execute motion to (x_{c+1}, y_{c+1})

5:     Measure $\overline{rsrp_{(x_c,y_c)}}$, update Path P

6:     Update M_{rsrp} using the GPR model based on P

7:     Select the next point (x_{c+2}, y_{c+2}) by minimizing the hybrid cost $c(P)$

8:     **if** $\overline{rsrp_{(x_{c+1},y_{c+1})}} < \tau = -140\,\text{dBm}$ **then**

9:         Rollback to the most recent safe point (x_c, y_c) and recalculate the path

10:    **else**

11:        $c \leftarrow c + 1$

12:    **end if**

13: **end while**

We will use the RSRP measurements obtained by the robot and GPR to predict large-scale and small-scale fading in unexplored areas, thereby obtaining more accurate Signal coefficient factor estimates.

In this section, we provide a detailed explanation of how to predict large-scale and small-scale fading. First, we describe how to denoise sampled RSRP data, which helps stabilize measurement variations and improve data reliability. Then, we introduce the concepts of large-scale and small-scale fading based on the RSS model, which is defined by path loss, shadowing, and multipath effects. Next, we demonstrate how to use measured

RSRP and GPR to predict large-scale fading, enabling more accurate RSRP estimations. Finally, we employ a spatial Bayesian method along with denoised RSRP values processed by the EWMA filter to predict small-scale fading and quantify the probability of network disconnection along the path.

4.1.1 Measured Data Processing and Denoising

Typically, RSRP measurements (in dBm) from wireless adapters are susceptible to noise and temporal fluctuations in addition to multipath fading. This noise can be mitigated by applying an Exponentially Weighted Moving Average (EWMA) filter [14].

In our method, we assume that the robot obtains 10 RSRP sampled datas each time it reaches a point. For any visited point in the set $\mathbf{D} = \{(x_i, y_i)\}_{i=0}^{N-1}$, each point $(x_i, y_i), i = 0, 1, \ldots, N-1$ receives 10 RSRP samples $\{rsrp_{(x_i,y_i)}^{(j)}\}_{j=1}^{10}$, which are processed using the EWMA filter:

$$rsrp_{(x_i,y_i)}^{(j)} = rsrp_{(x_i,y_i)}^{(j-1)} + \alpha\big(rsrp_{(x_i,y_i)}^{(j)} - rsrp_{(x_i,y_i)}^{(j-1)}\big), \tag{2}$$

where $rsrp_{(x_i,y_i)}^{(j)}$ represents the jth RSRP sampled data at point (x_i, y_i), and α is the smoothing factor.

To minimize the noise present in $\{rsrp_{(x_i,y_i)}^{(j)}\}_{j=1}^{10}$, we apply the EWMA filter to smooth the samples RSRP data, thereby enhancing data stability and reliability.

4.1.2 Radio Signal Strength Model

When a radio signal propagates from a source to a destination, its strength attenuation depends on environmental factors such as distance (path loss), objects in the environment (shadowing), and spatio-temporal dynamics (multipath fading) [14]. A frequently used model to represent the RSS is given by [15]:

$$RSS(d, t) = RSS_{d_0} - \underbrace{10\eta \log_{10}\left(\frac{d}{d_0}\right)}_{\text{Path Loss}} - \underbrace{\Psi(d)}_{\text{Shadowing}} - \underbrace{\Omega(d, t)}_{\text{Multipath}}, \tag{3}$$

where RSS_{d_0} is the RSS at a reference distance d_0 (usually $1\,\text{m}$), which depends on the transmit power, antenna gain, and the radio frequency used. η is the path loss exponent,

a propagation constant of the given environment. $d = \|(x, y) - (x_{\text{BS}}, y_{\text{BS}})\|$ is the distance of the receiver (at point (x, y)) from the radio source (at point $(x_{\text{BS}}, y_{\text{BS}})$). $\Psi \sim \mathcal{N}(0, \sigma)$ is a Gaussian random variable typically used to represent shadowing, while Ω is a Nakagami-m distributed variable representing multipath fading. Path loss and shadowing belong to large-scale fading. Large-scale fading refers to the slow attenuation of signal strength due to increased propagation distance and large obstacles (such as buildings, hills, terrain, etc.) that block or reflect the signal during propagation. Multipath $\Omega(d, t)$ belongs to small-scale fading. Small-scale fading refers to the rapid fluctuations in received signal strength over short time periods or small areas due to multipath propagation and channel variations. We focus on predicting and utilizing the RSRP rather than the RSS. RSS represents the total received signal power, while RSRP considers only the power from the reference base station. The key reason for this choice is that RSRP specifically measures the power of the reference signal transmitted by the base station, providing a more stable and accurate indicator of the radio channel conditions. In contrast, RSS typically includes the aggregate power of all received signals, which may encompass interference and noise components, leading to greater variability. Given that modern cellular networks (e.g., LTE and 5G) rely on RSRP for tasks such as cell selection and handover decisions, employing RSRP allows our model to better reflect the operational metrics used in these networks.

RSRP follows similar propagation characteristics to RSS, and we quantify the signal along the path from the perspectives of large-scale fading and small-scale fading.

In our method, the robot maintains an RSRP map, denoted as M_{rsrp}, where each unvisited location (x_*, y_*) is associated with a predicted RSRP value $rsrp'_{(x_*,y_*)} \in M_{\text{rsrp}}$. The value $rsrp'_{(x_*,y_*)}$ is computed using the proposed prediction method. Additionally, our method incorporates real-time sampled data. Whenever sampled data at an unvisited location (x_*, y_*) is obtained, we compute the measured average and update $rsrp'_{(x_*,y_*)}$ to reflect the measured mean.

First, we use ray-tracing simulation and prior BIM data to estimate $rsrp'_{(x_*,y_*)}$ for each unvisited location (x_*, y_*). In simple terms, ray-tracing simulation treats radio waves as numerous energy-carrying rays. These rays are traced to simulate radio wave interactions with obstacles, including reflection, refraction, and diffraction. The total energy of all rays reaching the Rx is then computed to obtain the predicted RSRP value.

In ray-tracing simulations, path loss and shadowing are accounted for, but multipath effects caused by dynamic obstacles cannot be estimated.

Since ray-tracing simulations cannot reflect the temporal variations in large-scale fading in real time (e.g., those induced by weather factors such as temperature and humidity), we adopt a prediction method based on sampled data and GPR to compensate for this limitation. Specifically, we first compute the difference between the measured average RSRP $\overline{rsrp_{(x_i,y_i)}}$ after arrival and the predicted RSRP $rsrp'_{(x_i,y_i)}$ before arrival, where $\overline{rsrp_{(x_i,y_i)}}$ is computed as the mean of the ten measured RSRP values $\{rsrp^{(j)}_{(x_i,y_i)}\}^{10}_{j=1}$.

This difference is then used to construct a GPR model to update the difference map $\Delta\mathcal{M}_{rsrp}$, which represents the difference between the measured and predicted values ΔRSRP at each location in the map.

Then, for an unvisited point (x_*, y_*), the updated ΔRSRP$_{(x_*,y_*)}$ values from $\Delta\mathcal{M}_{rsrp}$ are used to correct the predicted RSRP values, thereby obtaining the updated $rsrp'_{(x_*,y_*)}$.

Throughout the entire process, all subsequent data updates are applied to $rsrp'_{(x,y)}$. That is, whenever new sampled data become available, we employ the same prediction mechanism to update the values of $rsrp'_{(x,y)}$ in M_{rsrp}, ensuring that the map accurately and in real time reflects the current average power distribution and large-scale fading conditions in the area. Additionally, because ray-tracing simulations do not simulate small-scale fading effects [15], we estimate the signal fluctuations caused by multipath effects by predicting the parameters that determine the empirical distribution of small-scale fading. We also use GPR to predict small-scale fading at unvisited points. The specific implementation details will be described below.

4.1.3 Large-Scale Fading Prediction (Difference-Based Prediction)

Large-scale fading includes path loss and shadowing. Shadowing effects are due to the presence of large obstacles in the signal propagation path, leading to signal blockage or attenuation. This type of attenuation changes very slowly over time, but the daily level of attenuation and the attenuation at different locations can vary. For example, at the same location, attenuation on a rainy day differs from a sunny day; similarly, attenuation in a LOS path differs from a NLOS path. Figure 2 shows a radio attenuation map generated by a radio propagation simulation tool. The color scale from purple to red represents
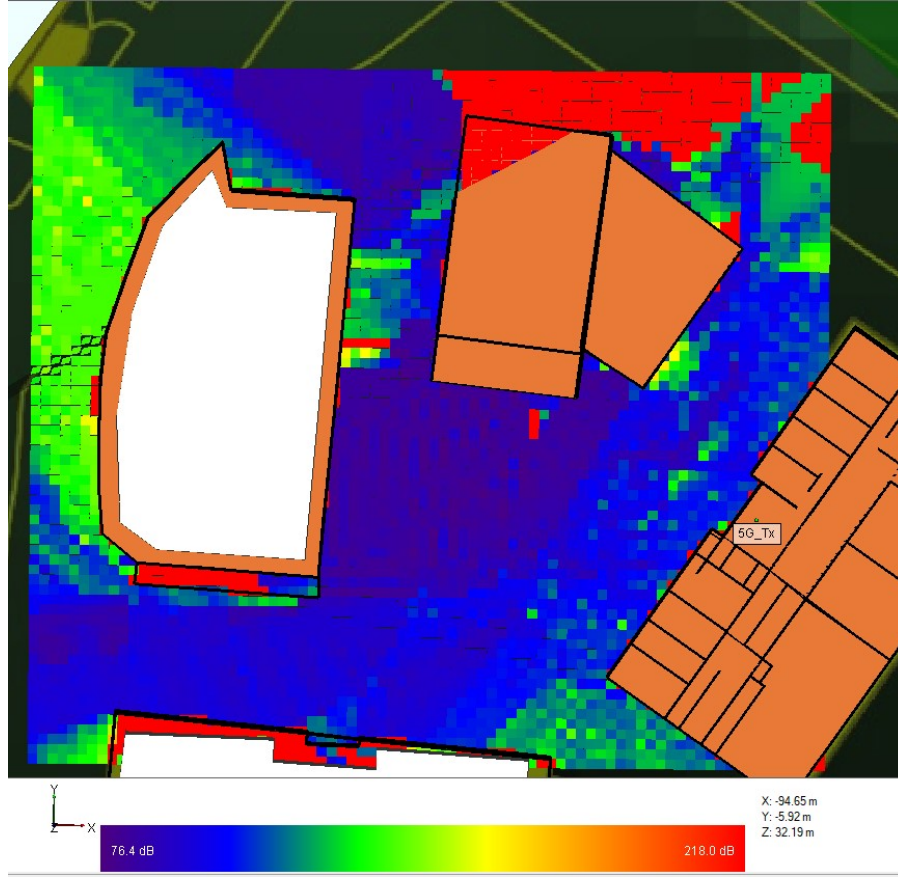
Figure 2: Large-scale fading. The colors from purple to red indicate attenuation levels from high to low.

attenuation levels from high to low. It can be observed that there are differences in the colors among the various regions in the Figure2, which indicates that the degree of fading varies across these areas. Since large-scale fading directly determines the measured average RSRP at each location, and our method aims to obtain more accurate RSRP predictions during navigation, it is necessary to model the large-scale fading for every potentially visitable point on the map.

When performing large-scale fading prediction, for any point on the visited points before reaching the target T, denoted as $\mathbf{D} = [(x_0, y_0), (x_1, y_1), \dots, (x_{N-1}, y_{N-1})]$, we have obtained the differences $\Delta\text{RSRP}_{(x_i, y_i)}$ between the measured average RSRP $\overline{rsrp_{(x_i, y_i)}}$ after arrival and the predicted RSRP at (x_i, y_i) before arrival, denoted as $rsrp'_{(x_i, y_i)}$. Thus, the differences $\Delta\text{RSRP}_{(x_i, y_i)}$ values are given by:

$$\Delta\text{RSRP}_{(x_i,y_i)} = rsrp'_{(x_i,y_i)} - \overline{rsrp_{(x_i,y_i)}}. \tag{4}$$

These difference data points form a set of visited point $\mathbf{D}$ used to establish a GPR model to update the difference map $\Delta\mathcal{M}_{rsrp}$. GPR is a non-parametric method for modeling a distribution over functions. Its fundamental assumption is that the function values at any finite set of points follow a joint Gaussian distribution. Since radio wave propagation follows a joint Gaussian distribution, we adopt GPR as a key component of our prediction method.

Suppose we have the difference map $\Delta\mathcal{M}_{rsrp}$, which contains the difference values of visited points and the predicted difference values of unvisited points. $\Delta\mathcal{M}_{rsrp}$ is obtained from the set of visited point $\mathbf{D}$ by calculating the difference between each averaged sampled data and its predicted value. The set of differences between the sampled averages and predicted values at each point in $\mathbf{D}$ as:

$$\mathbf{f} = [\Delta\text{RSRP}_{(x_0,y_0)}, \Delta\text{RSRP}_{(x_1,y_1)}, \dots, \Delta\text{RSRP}_{(x_{N-1},y_{N-1})}]^T.$$

For any unvisited point (x_*, y_*), the GPR assumes that the function value at (x_*, y_*) is jointly Gaussian with the set of visited point $\mathbf{D}$. We choose the Radial Basis Function (RBF) kernel function to capture the correlation between points in $\mathbf{D}$. The RBF kernel function defines the similarity between two spatial points (x, y) and (x', y'), which influences the covariance structure in GPR. The kernel function is given by:

$$k((x,y),(x',y')) = \sigma_f^2 \exp\left(-\frac{\|(x,y)-(x',y')\|^2}{2l^2}\right), \tag{5}$$

where l is the length-scale parameter, which controls how quickly the correlation decays with distance, and σ_f^2 is the signal variance. exp represents the exponential function. Its role is to convert the distance between two points (x, y) and (x', y') into a weight or similarity value between 0 and 1, thereby computing their covariance. The higher the correlation between two spatial points (x, y) and (x', y'), the closer the exponential function component in Equation 5 is to 1, meaning that $k((x,y),(x',y'))$ will output a value close to σ_f^2. In our method, the covariance matrix between points in

$\mathbf{D} = \{(x_0, y_0), (x_1, y_1), \dots, (x_{N-1}, y_{N-1})\}$ is used to compute the correlation between any of the visited points, given by:

$$\mathbf{K} = [k((x_i, y_i), (x_j, y_j))]_{i,j=0}^{N-1}. \tag{6}$$

We use the RBF kernel in Equation 6 to compute the correlation between the unvisited point (x_*, y_*) and any of the visited points, and store the results in the covariance matrix $\mathbf{k}_*$. The covariance matrix $\mathbf{K}$ of the visited locations and the set of differences $\mathbf{f}$ at the visited points are then used to calculate $\Delta\text{RSRP}_{(x_*, y_*)}$ and its variance $\text{Var}[\Delta\text{RSRP}_{(x_*, y_*)}]$ at the unvisited point (x_*, y_*):

$$\mathbf{k}_* = [k((x_*, y_*), (x_0, y_0)),$$

$$k((x_*, y_*), (x_1, y_1)), \dots, k((x_*, y_*), (x_{N-1}, y_{N-1}))]^T,$$

$$\Delta\text{RSRP}_{(x_*, y_*)} = \mathbf{k}_*^T \mathbf{K}^{-1} \mathbf{f},$$

$$\text{Var}[\Delta\text{RSRP}_{(x_*, y_*)}] = k((x_*, y_*), (x_*, y_*)) - \mathbf{k}_*^T \mathbf{K}^{-1} \mathbf{k}_*. \tag{7}$$

Using the GPR prediction, we obtain the predicted difference $\Delta\text{RSRP}_{(x_*, y_*)}$ for areas not yet visited. Based on this, we update the RSRP map M_{rsrp} with the data at this point, $rsrp'_{(x_*, y_*)}$:

$$rsrp'_{(x_*, y_*)} = rsrp'_{(x_*, y_*)} - \Delta\text{RSRP}_{(x_*, y_*)}. \tag{8}$$

Thus, we obtain a large-scale fading map that more closely approximates the true average RSRP value. During navigation, we use $rsrp'_{(x_*, y_*)}$ at unvisited locations in M_{rsrp} to plan the path. Therefore, an accurate estimate of $rsrp'_{(x_*, y_*)}$ is directly related to maintaining network connection.

4.1.4 Small-Scale Fading Prediction (Nakagami-m Parameter Prediction)

Small-scale fading refers to the rapid fluctuations in received signal strength over short time periods or small areas due to multipath propagation and channel variations. Unlike large-scale fading (such as path loss and shadowing), small-scale fading is caused by reflection, diffraction, and scattering in the environment, resulting in signals arriving at the receiver
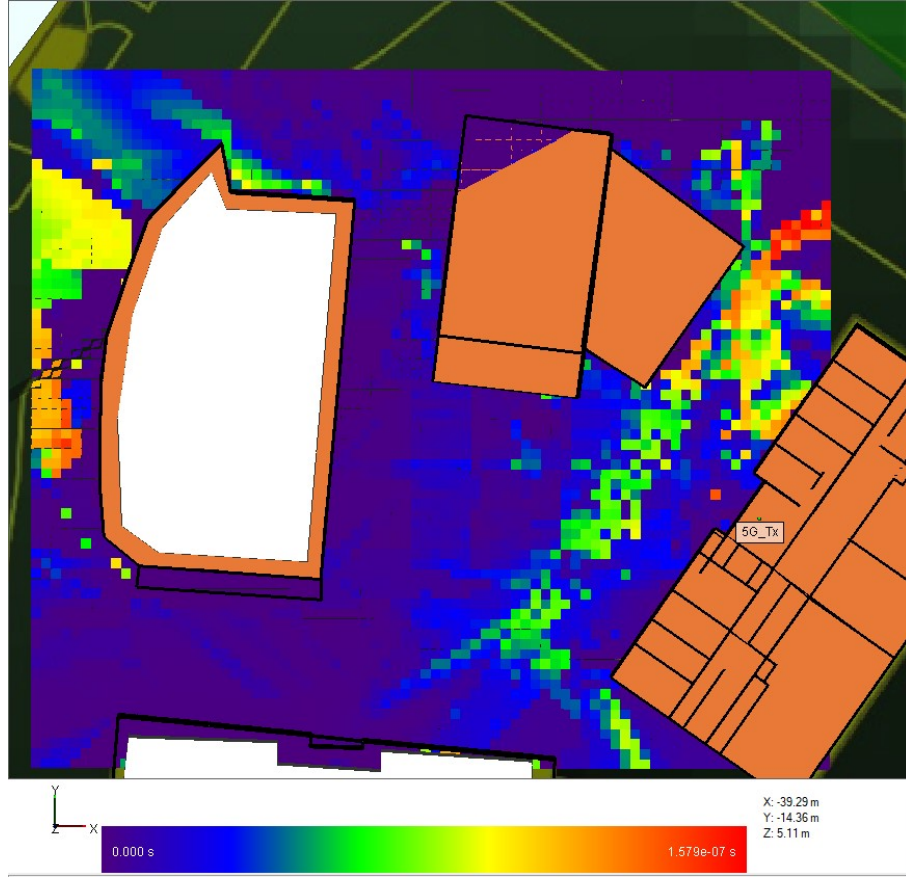
Figure 3: Delay spread: the difference in signal propagation times of different paths. Colors from purple to red indicate delay levels from high to low.

via multiple paths. Figure 3 shows the delay spread. Areas with high delay spread typically indicate a more complex multipath propagation environment and are more susceptible to fast fading. One can see that the delay spread at each point differs, and even adjacent points can have very large differences. This may result in different network fluctuations at adjacent locations, thereby increasing the risk of disconnection. In order to ensure that the robot maintains a safer network quality at all potentially visitable points, it is necessary to model small-scale fading.

For small-scale fading prediction, we need to calculate the probability of disconnection at each unvisited location (x_*, y_*) to quantify small-scale fading. We choose the Nakagami-m distribution to model signal fluctuations. The sampled data obtained at visited locations in $\mathbf{D} = [(x_0, y_0), (x_1, y_1), \ldots, (x_{N-1}, y_{N-1})]$ can be used to fit the Nakagami-m distribution

parameters at the unvisited point (x_*, y_*), including the shape parameter m and the average power Ω.

We apply a spatial Bayesian method to predict m. Based on the set of 10 sampled RSRP datas at each visited point $(x_i, y_i)_{i=0}^{N-1}$ in $\mathbf{D}$, denoted as

$$\mathcal{R}(x_i, y_i) = \{rsrp_{(x_i,y_i)}^{(1)}, rsrp_{(x_i,y_i)}^{(2)}, \ldots, rsrp_{(x_i,y_i)}^{(10)}\},$$

we use Bayesian inference and the Maximum A Posteriori (MAP) method to fit the Nakagami-m distribution parameter m. Then, we apply GPR to predict $m_{(x_*, y_*)}$ at unvisited locations (x_*, y_*) using the fitted values of m at visited locations (x_i, y_i), denoted as $\mathbf{m} = [m_{(x_0,y_0)}, m_{(x_1,y_1)}, \ldots, m_{(x_{N-1}, y_{N-1})}]$.

To estimate the shape parameter m in the Nakagami-m distribution at each point (x_i, y_i) in $\mathbf{D}$, we utilize Bayesian inference based on the RSRP sampled datas $\{rsrp_{(x_i,y_i)}^{(j)}\}_{j=1}^{10}$. Specifically, the 10 RSRP samples at each location are first converted into the corresponding received signal amplitudes $\{r_{(x_i,y_i)}^{(j)}\}_{j=1}^{10}$. These values are then used to compute the likelihood function under the Nakagami-m model:

$$r_{(x_i,y_i)} = \left\{ \sqrt{10^{\frac{rsrp_{(x_i,y_i)}^{(j)}}{10}}} \mid rsrp_{(x_i,y_i)}^{(j)} \in \mathcal{R}(x_i, y_i) \right\},$$

$$p(\mathcal{R}(x_i, y_i); m_{(x_i,y_i)}, \Omega) = \prod_{j=1}^{10} \frac{2\, m_{(x_i,y_i)}^{m_{(x_i,y_i)}}}{\Gamma(m_{(x_i,y_i)})\, \Omega^{m_{(x_i,y_i)}}} r_{(x_i,y_i)}^{(j)\,2m_{(x_i,y_i)}-1} \exp\left(-\frac{m_{(x_i,y_i)}}{\Omega}(r_{(x_i,y_i)}^{(j)})^2 \right),$$

$$(9)$$

where $\Gamma(m(x_i, y_i))$ represents the value of the Gamma function evaluated at $m(x_i, y_i)$. It is used to adjust the amplitude of the entire distribution so that the total probability over all possible signal amplitudes is equal to 1. Ω represents the scale parameter, which corresponds to the average power of the signal, i.e., $\Omega = \mathbb{E}[r^2]$, where r is the received signal amplitude.

The amplitudes of the 10 RSRP samples $\{r_{(x_i,y_i)}^{(j)}\}_{j=1}^{10}$ measured at the visited locations $(x_i, y_i)_{i=0}^{N-1}$ conform to the posterior distribution at these points. Therefore, we first compute the overall likelihood function $\mathcal{L}(m)$, which represents the joint probability of these samples given a specific value of the parameter m. In other words, $\mathcal{L}(m)$ measures how

well the parameter m fits these sampled data, serving as the basis for subsequent Bayesian estimation and MAP estimation.

Assuming that the prior distribution of $m_{(x_i,y_i)}$ follows a Gamma distribution, we update the prior distribution using a Bayesian method. Finally, we perform MAP estimation to maximize the likelihood of $\mathcal{L}(m)$ under the posterior distribution. This allows us to obtain a posterior distribution that incorporates as many of the observed amplitudes $\{r^{(j)}_{(x_i,y_i)}\}^{10}_{j=1}$ as possible. Consequently, we obtain the shape parameter m at the visited locations $(x_i, y_i)^N_{i=0}$ as the set $\mathbf{m} = [m_{(x_0,y_0)}, m_{(x_1,y_1)}, \ldots, m_{(x_N,y_N)}]$. The specific formula is as follows:

$$\mathcal{L}(m_{(x_i,y_i)}) = \prod_{j=1}^{10} p(r^{(j)}_{(x_i,y_i)}; m_{(x_i,y_i)}, \Omega_{(x_i,y_i)}), \tag{10}$$

$$p(m_{(x_i,y_i)}) = \frac{\beta^\alpha}{\Gamma(\alpha)} m_{(x_i,y_i)}^{\alpha-1} e^{-\beta m_{(x_i,y_i)}}, \quad m_{(x_i,y_i)} > 0, \tag{11}$$

$$p(m_{(x_i,y_i)}|\mathbf{D}) \propto \mathcal{L}(m_{(x_i,y_i)}) \, p(m_{(x_i,y_i)}), \tag{12}$$

$$m_{\text{MAP}} = \arg \max_{m_{(x_i,y_i)}} \Big(\mathcal{L}(m_{(x_i,y_i)}) \, p(m_{(x_i,y_i)}) \Big). \tag{13}$$

Similarly, we apply GPR to the shape parameters $m_{(x_i,y_i)}$ obtained at visited locations (x_i, y_i) to predict the m value at an unvisited location (x_*, y_*). Given the fitted shape parameters at visited locations, denoted as $\mathbf{m} = [m_{(x_0,y_0)}, m_{(x_1,y_1)}, \ldots, m_{(x_{N-1},y_{N-1})}]$, we perform a spatial interpolation prediction for m using GPR:

$$m_{(x_*,y_*)} = \mathbf{k}_*^T \mathbf{K}^{-1} \mathbf{m}, \tag{14}$$

$$\text{Var}[m_{(x_*,y_*)}] = k((x_*, y_*), (x_*, y_*)) - \mathbf{k}_*^T \mathbf{K}^{-1} \mathbf{k}_*, \tag{15}$$

where $\mathbf{m} = [m_{(x_0,y_0)}, m_{(x_1,y_1)}, \ldots, m_{(x_{N-1},y_{N-1})}]^T$. Through this process, we do not need to directly measure the Nakagami-m parameters in unvisited areas. Instead, we can reasonably predict m for unknown regions based on the known parameters and the Euclidean distance relationships between coordinates.

Next, we use the predicted $m_{(x_*,y_*)}$ at the unvisited location (x_*, y_*) along with the predicted value $rsrp'_{(x_*,y_*)}$ to estimate the probability of disconnection at that location.

First, we model the Nakagami-m distribution at (x_*, y_*) using $m_{(x_*, y_*)}$ and the predicted $rsrp'_{(x_*, y_*)}$. Then, we compute the probability that the $rsrp'_{(x_*, y_*)}$ falls below the threshold - 140dBm using the cumulative distribution function (CDF) of the Nakagami-m distribution. Since the CDF requires power values in linear scale, we convert the predicted RSRP $rsrp'_{(x_*, y_*)}$ from dBm to Watts, denoted as $r'_{(x_*, y_*)}$, also convert the threshold $\tau =$ - 140 dBm from dBm to Watts, denoted as r_{th}:

$$r'_{(x_*, y_*)} = 10^{\frac{rsrp'_{(x_*, y_*)} - 30}{10}} \text{ (Watt)},$$

$$\rho(x_*, y_*) = F_{\text{Nakagami}}\Big(\tau;\, m_{(x_*, y_*)},\, r'_{(x_*, y_*)}\Big)$$

$$= \frac{\gamma\Big(m_{(x_*, y_*)},\, \dfrac{m_{(x_*, y_*)}}{r'_{(x_*, y_*)}}\, r_{\text{th}}^2\Big)}{\Gamma\big(m_{(x_*, y_*)}\big)}. \tag{16}$$

Finally, for the unvisited location (x_*, y_*), we have updated the values of $rsrp'_{(x_*, y_*)}$ in M_{rsrp} and the predicted $m_{(x_*, y_*)}$. Thus, we can construct a Nakagami-m distribution to predict the probability that RSRP falls below the threshold $\tau = -140\,\text{dBm}$, denoted as $\rho(x_*, y_*)$.

4.2 Navigation Method Integrating Signal coefficient factor and Distance Cost

We utilize Signal coefficient factor derived from ray-tracing simulations, GPR, and spatial Bayesian inference, combined with Distance Cost, to plan and execute a path to target T.

In this section, we first introduce the cost function used in our method, which integrates both Signal coefficient factor and Distance Cost. This cost function normalizes the RSRP cost and disconnection probability within the Signal coefficient factor component, allowing these two costs to be adjusted based on scenario-specific weighting coefficients. This flexibility enables adaptation to different requirements.

Furthermore, for RSRP cost, we divide the RSRP into two regions. Compared to a linear division, our method makes the RSRP cost more sensitive to values below the threshold while remaining less responsive to values above the threshold.

Finally, we explain how, in cases where the robot navigates into a region with RSRP below the threshold due to inaccurate predictions, the GPR update process and path

recalculation procedure are performed to adaptively correct the navigation.

4.2.1　Cost Function

In our method, the overall path cost is minimized by minimizing the cost between each point. Specifically, at each step the method selects the next point (x_{i+1}, y_{i+1}) such that the incremental cost $c((x_i, y_i), (x_{i+1}, y_{i+1}))$ is minimized, ensuring that the cumulative cost of the path to reach the target T is as low as possible. the optimal path $\{(x_i, y_i)\}_{i=0}^{N-1}$ from start point S to target point T is computed by minimizing the total cost $c(S, T)$, which is expressed as the sum of the costs between each pair of consecutive points:

$$c(S, T) = \sum_{i=0}^{N-1} c((x_i, y_i), (x_{i+1}, y_{i+1})). \tag{17}$$

The cost function $c : C \times C \to \mathbb{R}$ is defined to combine both disconnection probability predictions and RSRP predictions. Specifically, it is given by:

$$c((x_i, y_i), (x_{i+1}, y_{i+1})) = (d((x_i, y_i), (x_{i+1}, y_{i+1})) + h(x_{i+1}, y_{i+1})) \cdot$$
$$(\lambda_1 \pi(x_{i+1}, y_{i+1}) + \lambda_2 \rho(x_{i+1}, y_{i+1})). \tag{18}$$

$$\pi(x_i, y_i) = \begin{cases} \epsilon + 0.2 \left(\dfrac{-70 - rsrp'_{(x_i, y_i)}}{50} \right), & \text{if } rsrp'_{(x_i, y_i)} \geq -120, \\ 0.2 + 0.8 \left(\dfrac{-120 - rsrp'_{(x_i, y_i)}}{130} \right), & \text{otherwise.} \end{cases} \tag{19}$$

$$\rho(x_i, y_i) = F_{\text{Nakagami}}(10^{\frac{\tau - 30}{10}}; m_{(x_i, y_i)}, 10^{\frac{rsrp'_{(x_i, y_i)} - 30}{10}}). \tag{20}$$

The symbols used in the cost function are defined in Table 1. The equation18 combines the distance metric and the heuristic function, which depends on the distance to the target. The term $rsrp'_{(x_{i+1}, y_{i+1})}$ represents the predicted RSRP value at the next point (x_{i+1}, y_{i+1}), calculated through ray-tracing simulations and GPR. In wireless communication systems the RSRP value covers multiple levels: in close proximity to the base station or in favorable environmental conditions, the RSRP can reach around - 70 dBm, indicating strong signal quality. When the signal attenuates to approximately - 120 dBm, the device may be at the edge of network coverage, resulting in degraded connection quality. If the RSRP falls below - 140 dBm, the signal becomes extremely weak, making it difficult for the device to maintain a reliable connection, potentially leading to disconnection. An RSRP of - 250 dBm will inevitably result in a complete loss of connection.

So We assume that $rsrp'_{(x_i, y_i)}$ ranges within [- 70dBm, - 250dBm]. To ensure that the influence of the RSRP cost $\pi(x_i, y_i)$ and the disconnection probability $\rho(x_i, y_i)$ on path selection is balanced,

Table 1: Definition of variables in the cost function.

Symbol	Description
$d((x_i, y_i), (x_{i+1}, y_{i+1}))$	Euclidean distance between consecutive points.
$h(x_{i+1}, y_{i+1})$	Heuristic function estimating the remaining distance to the target.
$\pi(x_i, y_i)$	Normalized RSRP cost function.
$\rho(x_i, y_i)$	Probability that $rsrp'_{(x_i, y_i)}$ falls below the threshold $\tau = -140\,\text{dBm}$, computed via the Nakagami-m CDF.
$rsrp'_{(x_i, y_i)}$	Predicted RSRP value at (x_{i+1}, y_{i+1}) obtained from our prediction method.
$\lambda_1, \lambda_2 \in \mathbb{R}^+$	Weighting factors for RSRP cost and disconnection probability.
$\tau = -140\,\text{dBm}$	Critical RSRP threshold for connection loss.
$\epsilon = 10^{-6}$	A small value to prevent $\pi(x_i, y_i)$ from being zero.

we normalize both terms. Since $\rho(x_i, y_i) \in [0, 1]$ is already normalized, we apply a normalization process to $\pi(x_i, y_i)$.

The function $\pi(x_i, y_i)$ employs a piecewise linear mapping that divides the RSRP values into two regions: for RSRP values greater than or equal to - 120 dBm (i.e., the stronger signal region), a smoother mapping is applied, where each 1 dBm change corresponds to a small increment in $\pi(x_i, y_i)$, with a range of $[\epsilon, 0.2 + \epsilon]$. For RSRP values below - 120 dBm (i.e., the weaker signal region), a steeper mapping is used, where each 1 dBm decrease results in a significant increase in $\pi(x_i, y_i)$, with a range of $(0.2 + \epsilon, 1 + \epsilon]$. This design ensures that when the signal is weak, cost changes are more sensitive, making the navigation more likely to avoid points below the threshold. Conversely, for points with strong signals, cost variations are less significant, thereby reducing the impact of $\pi(x_i, y_i)$ on path selection for points above the threshold.

The weight λ_1 is used to adjust the influence of $\pi(x_{i+1}, y_{i+1})$ in the cost function.

Finally, $\rho(x_i, y_i)$ represents the probability of disconnection at the next point, calculated using the CDF of the Nakagami-m distribution based on whether $rsrp'_{(x_{i+1}, y_{i+1})}$ falls below the threshold τ. The weight λ_2 is used to adjust the influence of $\rho(x_i, y_i)$ in the cost function.

The Nakagami-m distribution is chosen for its ability to model both LOS and NLOS conditions through the shape parameter m. Specifically, $m \geq 1$ represents LOS scenarios with milder fading, while $m < 1$ captures NLOS scenarios with severe multipath effects. Compared to fixed-threshold methods that deterministically disconnect when sampled RSRP less than the threshold τ, our probabilistic model provides a finer-grained risk assessment by accounting for fading dynamics. For example, two paths with the same average RSRP but different fading characteristics (LOS vs. NLOS) can now be distinguished based on their disconnection probabilities. Mathematically, this is reflected in the Nakagami-m CDF: for a fixed RSRP threshold τ,

$$F_{\text{Nakagami}}(\tau; m_{\text{NLOS}}, \Omega) > F_{\text{Nakagami}}(\tau; m_{\text{LOS}}, \Omega) \quad \text{when} \quad m_{\text{NLOS}} < m_{\text{LOS}}. \tag{21}$$

Consequently, paths through LOS regions inherently exhibit lower $\rho((x_i, y_i))$ values for the same RSRP. By weighting $\rho(x_i, y_i)$ heavily in the cost function via λ_2, the navigation method prioritizes LOS routes, thereby reducing disconnection risks without solely relying on absolute RSRP value. When the prediction error of $rsrp'_{(x_i, y_i)}$ is large, the robot may unexpectedly enter a region where the RSRP falls below the threshold. This could result in a loss of network connectivity. To ensure a reliable network connection, the robot needs to retreat to the nearest point where the RSRP is above the threshold. Upon reaching this point, the path will be recalculated, and the robot will proceed towards the destination, repeating this process until it successfully reaches the target point.

5 Evaluation: Simulation Setup and Performance Analysis of the Proposed Navigation Method

5.1 Simulation Validity

To evaluate the performance of the proposed method, it is necessary to measure RSRP data across all locations on the map simultaneously to obtain correct RSRP values. However, conducting measurements at all locations simultaneously would require a significant cost. Therefore, we use the *Wireless InSite* simulation software, employing the ray-tracing method for wireless signal propagation simulation.

Apart from the parameters of the AP, the two key factors influencing the ray-tracing simulation are the geometric structure of buildings and the material properties of the environment. To ensure that the RSRP values used in the evaluation closely resemble those in the real environment, we refined the BIM in *Wireless InSite* based on the geometric structure and material properties of the Graduate School of Information Science and Technology (IST) building model at Suita Campus, Osaka University. This refinement helps obtain simulated values that are as close to the real environment as possible.

Additionally, we conducted real-world measurements at multiple locations around the IST building. To obtain data that closely approximates measurements taken at the same time, we performed multiple measurements at different dates but at the same time period under clear weather conditions. The distribution of measured RSRP values across different dates and corresponding time periods was used to calibrate the *Wireless InSite* simulation results. After calibration, the simulated RSRP values at corresponding locations were found to be close to the peak of the real-world RSRP distribution, indicating that the simulation results align well with actual measurements.

Since the simulation environment does not include moving obstacles such as pedestrians and vehicles, small-scale fading may be more significant in real-world scenarios. However, in the navigation task, the overall signal trend is more important than instantaneous signal variations. Therefore, the simulation method remains applicable to this study.

In the section (5.2), we will use the *Wireless InSite* simulation results as the correct RSRP values for configuring the robot's navigation experiment. Additionally, for fitting the Nakagami-m distribution required for real-world measurements during robot movement, we will use the measurement data obtained from multiple locations at IST to fit the Nakagami-m distribution. The fitted m values will then be interpolated spatially to estimate m at all points on the map. The value of m represents the degree of signal fading in the space. Since signal fading exhibits spatial correlation, spatial interpolation is a suitable method for estimating m values across the map.

In summary, the evaluation in this study will use the *Wireless InSite* simulated RSRP as the correct RSRP and the spatially interpolated fitted m as the correct m.

5.2 Experimental Configuration

To evaluate the performance of the proposed method, we conducted a series of simulation experiments using the *Wireless InSite* simulation software, employing the ray-tracing method for wireless signal propagation simulation. In our *Wireless InSite*[16] simulation environment, the

Table 2: Experiment Environment and Parameters

Experiment Parameters	
Environment	IST building model in Suita campus of Osaka University
5G AP Parameters	
Carrier frequency	4.85 GHz, Bandwidth: 100 MHz
AP transmit power	36.6 dBm
Height	19.8 m
Location	IST - A 6F
***Wireless InSite* Parameters**	
Simulation method	Ray-tracing
Grid spcing	0.5m
Grid height	1.4m
Robot Parameters	
Velocity	$V_{\max} = 0.5$ m/s
Height	1.4 m

space is modeled as a 3D grid pattern, divided into equal cubes, each representing a point. Each cube has a side length of 0.5 m, with its center positioned at a height of 1.4 m above the ground. When *Wireless InSite* calculates the RSRP at each point, it employs the ray-tracing method, which decomposes the signal into numerous rays and computes their refraction, reflection, and diffraction

at obstacles. The simulated RSRP value at each point is obtained by summing the energy of all rays reaching the corresponding cube.

As the robot traverses each cube, it collects RSRP measurements from a circular RSRP measurement area. Given that the robot moves at a maximum velocity of $V_{\max} = 0.5$ m/s and the diameter of the RSRP measurement area is 0.5 m, while RSRP is measured every 0.1 s, the robot can acquire 10 RSRP measurements for each cube it passes through. Figure 4 illustrates this process in a 2D schematic.

In our experiment, we simplify the 3D grid to a 2D grid, ignoring height variations of the robot within the map. If the robot has the capability to ascend or descend, our method can be extended by replacing the 2D coordinates in the set of visited points, $\mathbf{D} = [(x_0, y_0), (x_1, y_1), \ldots, (x_{N-1}, y_{N-1})]$, with 3D coordinates and updating the GPR accordingly. Therefore, we consider the 2D grid simplification sufficient for validating our approach.

The plan view position of the AP is located in the lower left of Figure 6. We conducted simulations around IST using the parameters in Table 2 and the BIM model in Figure 5, with the results shown in Figure 6. Different colors in Figure 6 represent different RSRP intensities.

The RSRP values transition from weak to strong, represented by a color gradient. In the weakest regions, the RSRP is shown in purple to green, corresponding to approximately -140 dBm. As the RSRP increases, it shifts to yellow, around -120 dBm. In areas with very strong RSRP, the color turns red, indicating an RSRP of approximately -80 dBm.

We use the RSRP data at each coordinate point in Figure 6 as the correct RSRP for evaluating our method.

The reason for choosing IST area is that RSRP on the plaza side and the road side of IST-C varies significantly, with the plaza side having good RSRP and the road side having poor RSRP. This setup allows us to verify that when only Distance Cost is considered, the robot may traverse the road side with poor RSRP, leading to disconnection. In contrast, when Signal coefficient factor is taken into account, the robot will detour to the plaza side with better RSRP, thereby maintaining continuous network connectivity.

5.3 Evaluation Scenarios

We evaluated the proposed method using a set of start and end points around IST-C and a Building Information Modeling (BIM) model with correct shape and height but incorrect material.

This BIM model simulates an environment where the geometric structure is accurate, but the material properties are not, allowing us to assess whether our method can still obtain paths with good RSRP despite inaccuracies in environmental information.
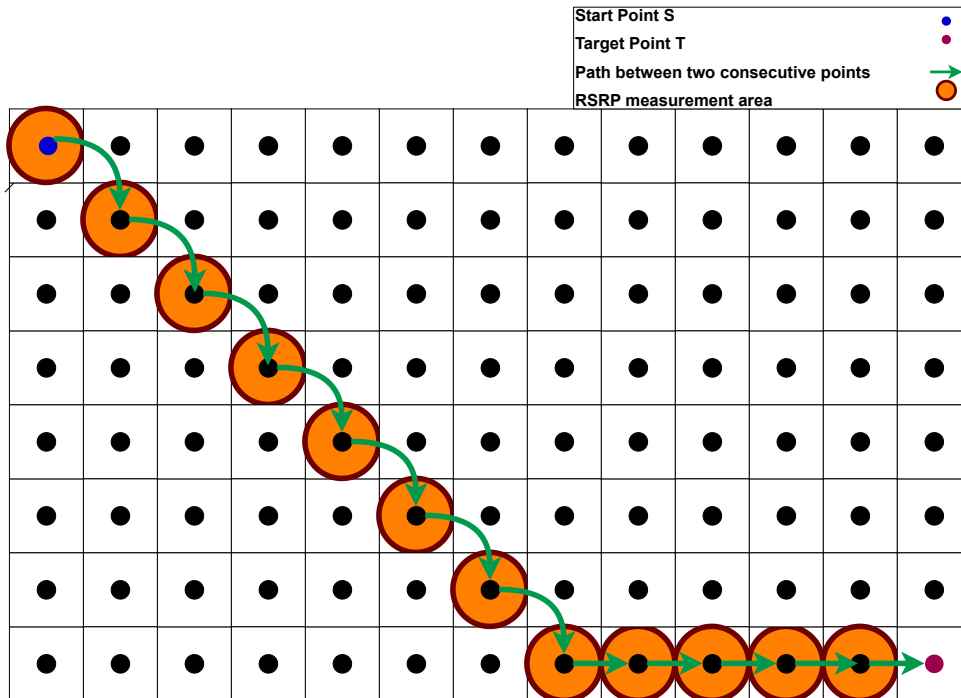
Figure 4: A 2D schematic representation of the robot moving from the start point S to the target point T in an obstacle-free environment while measuring RSRP within the RSRP measurement area. Blue dots represent the start point S, red dots represent the target point T, green arrows indicate the path between consecutive points, and orange circles denote the RSRP measurement area.

Figure 7 shows the prior RSRP data available to the robot at the start point. As the robot proceeds, this RSRP data is updated. By comparing with Figure 5, it is evident that there are regions in the map where color transitions are gradual and others where sudden changes occur. These differences indicate how RSRP varies in different areas. We aim to use Figure 7 to verify that our method can capture gradually varying RSRP using ray-tracing simulation and GPR. In contrast, where abrupt changes in RSRP occur, our method will revert to a safe location, update the RSRP information on the map, and replan the path.

5.4 Evaluation Metrics

We compare three distinct navigation strategies:
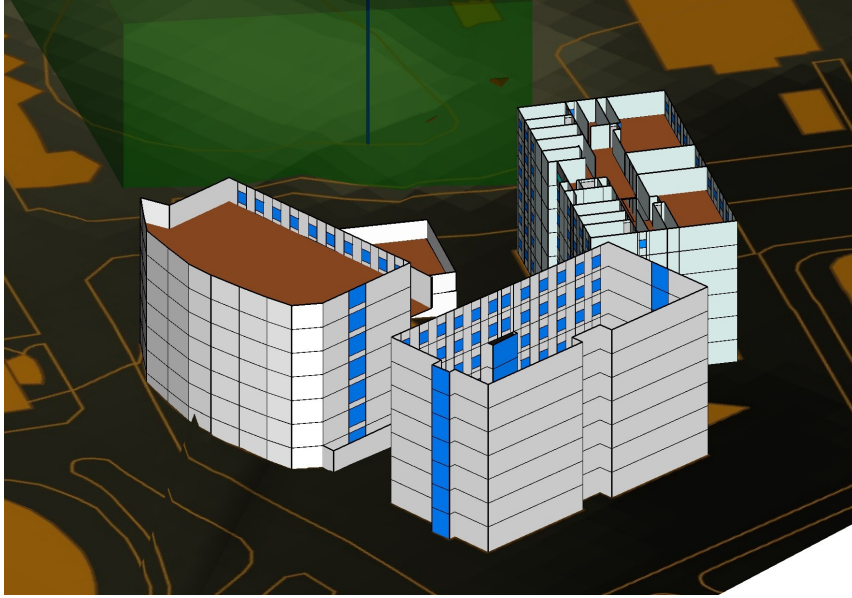
Figure 5: Experimental Environment: IST-C model in Wireless InSite with correct shape and height but correct material (3D view)RSRP distribution in the experimental environment (plan view),

For the comparison of these three navigation strategies, we focus on two aspects: the number of steps required to complete each path (i.e., Distance Cost) and the observed RSRP along the path. By comparing Distance Costs, we aim to confirm whether our method with only partial signal knowledge can achieve similar path choices to the full-information navigation, thereby demonstrating that signal safety is maintained with minimal path-length penalties. By comparing the observed RSRP in each strategy, we aim to show that our method maintains the signal above $-120\,\mathrm{dBm}$ (i.e., strong signal) most of the time, thus achieving the target of ensuring robust connectivity.

Finally, we will also discuss the line plots of observed and predicted RSRP along the route, mapping specific sections of these plots to their corresponding locations in the environment. This analysis will clarify how our method handles signal variations observed in the real world.

In subsequent comparative figures: From Figures 9 and 10, we observe that baseline distance-based method produces the shortest route but includes portions where the RSRP falls well below the threshold τ, risking network disconnection. The RSRP optimized method, which has complete and correct RSRP data, detours around areas of weak signal. Because the AP is located near the coordinates $(-30, -60)$ in Figure 9, RSRP optimized method cost function results in a route that is longer than the baseline method direct path. Notably, more than 80% of the RSRP optimized
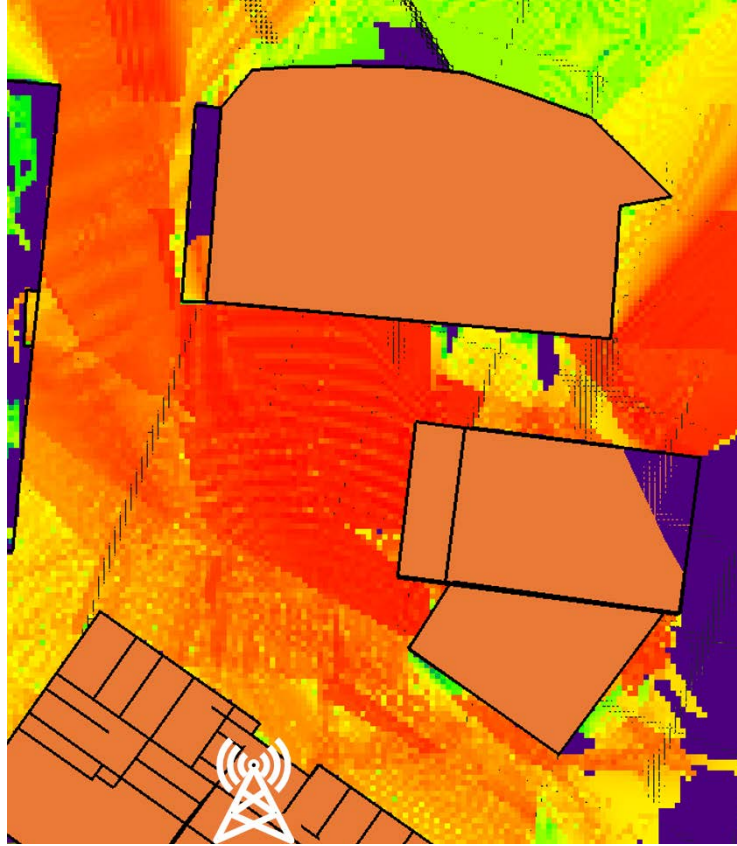
Figure 6: RSRP distribution in the experimental environment (plan view). RSRP increases from weak.

method receives excellent signal levels (between $-80\,$dBm and $-100\,$dBm).

Our proposed Method, which starts with the prior RSRP data shown in Figure 7albeit inaccurate and uses GPR for navigation, also detours similarly to the RSRP optimized method, indicating that our method correctly captures the differences in RSRP on each side of the buildings. However, the Distance Cost for our method is slightly longer than both RSRP optimized method and baseline distance-based method, because the robot must occasionally explore and even backtrack to ensure a safe network connection due to the initial inaccuracies in the prior RSRP data. Nonetheless, from the our method in Figure 10, we see that our method maintains RSRP above the threshold τ in almost all cases even in a complex environment like IST. Specifically, in our experimental scenario, the final Distance Cost was 213 steps, with only two points having observed RSRP below τ. This demonstrates that our method can accurately capture signal variations in the environment, ensuring that more than 99% of the path stays above the threshold τ despite limited prior information.
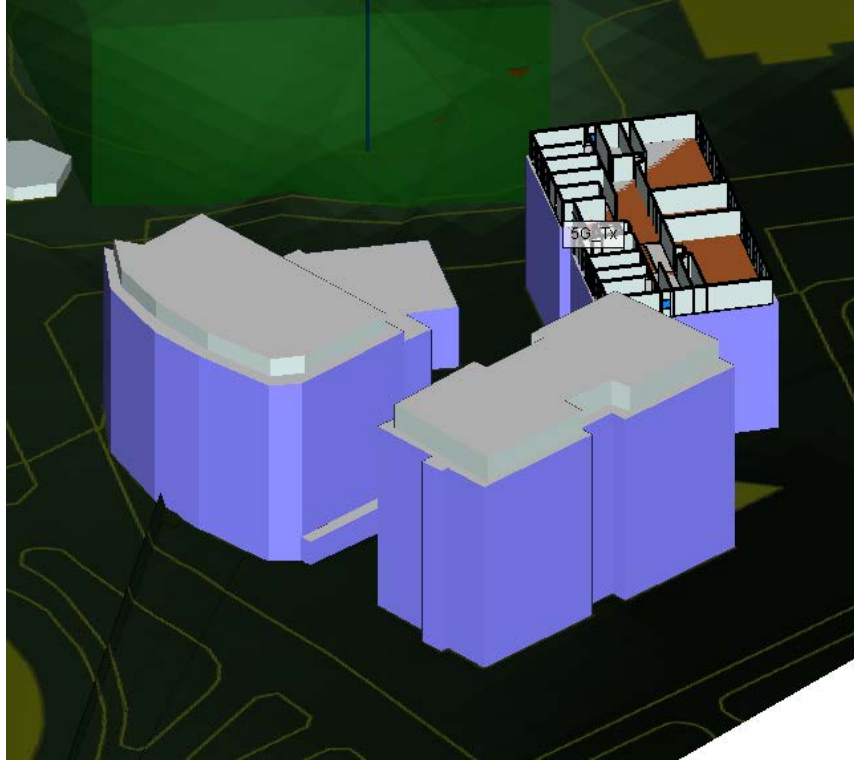
Figure 7: Evaluation Environment: IST model in Wireless InSite with correct shape and height but incorrect material (3D view),

Figure 11 shows both the predicted and observed RSRP values for our method along the path. The blue line indicates the GPR-based predictions (supported by ray-tracing simulation), while the yellow line indicates actual observed values measured by the robot.

In Figure 12, the pale blue shaded region $(0-30$ steps) on the path corresponds to the lower blue zone in the left model figure, and similarly for the purple and black zones. Across these three segments, the predicted and observed RSRP values exhibit small errors, and the path advances smoothly, indicating that the robot's predictions and observations are closely aligned. This outcome suggests that our method — combining ray-tracing simulation with GPR — accurately captures signal patterns along these parts of the route. The blue zone is near the start point, where the amount of sampling data is initially limited. Since the prediction accuracy of GPR is directly related to the amount of sampling data, one might expect lower accuracy near the start. However, the small error in the blue region's observed and predicted values confirms that the ray-tracing simulation provides a strong initial estimate at the start. As more samples accumulate, we see similarly small prediction errors in the purple and black regions, suggesting that the GPR method captures the gradual, uniform changes in RSRP within these areas. In Figure 14, the green and
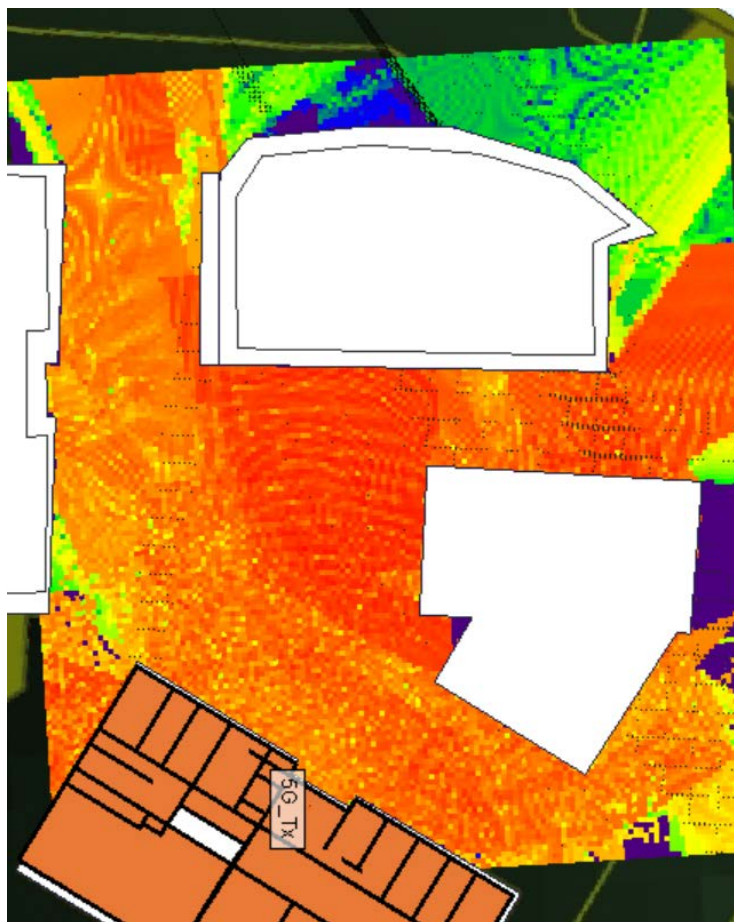
Figure 8: Evaluation Environment: RSRP distribution in the experimental environment (plan view).

black zones in the path have larger differences between predicted and observed RSRP. In these areas, the path exhibits detours and backtracking, and in some cases the observed RSRP even dips below the threshold τ. This indicates that the prior RSRP data in these regions differed significantly from the actual signal conditions, so our method's initial predictions did not fully capture the local signal variation.

From the Gree zone in Figure15, we see that although the colors of the observed data and the prior map are somewhat similar, they differ in gradient trends. This suggests that both predicted and observed RSRP may still be strong, yet local discrepancies arise in the direction or rate of change, which disrupts the GPR updates. Since our GPR method relies on differences between predicted and observed values to refine the model, an uneven pattern of differences can reduce predictive performance in that zone.

In the black zone in Figure14, by contrast, the color in the prior data deviates considerably

Table 3: Comparison of Different Navigation Methods

Method	Description
Method 1 (Blue Line)	A baseline method using purely distance-based optimization. Its cost function only minimizes Distance Cost and ignores RSRP considerations.
Method 2 (RSRP optimized method)	A theoretical optimum that assumes perfect prior knowledge of signal distribution. Its cost function optimizes RSRP across the entire trajectory.
Method 3 (Yellow Line)	Our proposed method, which employs GPR to estimate unknown RSRP values dynamically. A safety-oriented cost function penalizes any signal below the viability threshold of $-140\,\mathrm{dBm}$ while also optimizing path efficiency.

from the actual observations, and the color transitions are abrupt rather than smooth. This indicates a dramatic change in signal levels within these areas, where GPR tends to have difficulty capturing such sudden variations. Even so, our method ultimately finds a safe signal path through additional detours and exploration, demonstrating that it can still perform effectively in regions of sharp signal fluctuations. Ray-tracing simulation requires an environmental model and detailed information of the base stations as inputs to calculate signal propagation. In the method that solely uses ray-tracing simulation, we use the model from Fig. 7 as the input; the AP are the same as those used in our method, and the cost function is identical. Navigation is ultimately performed based on the RSRP data computed by the ray-tracing simulation.

In Figure 16 as seen from the paths generated by the two methods, the ray-tracing simulation-based method also chooses to detour around buildings , that is, to navigate along the side with better RSRP. In blue area there are segments where the paths produced by the ray-tracing simulation-based method and our method overlap , which indicates that even if the material properties of the environmental model are inaccurate, the ray-tracing simulation can still capture signal propagation to a certain extent.

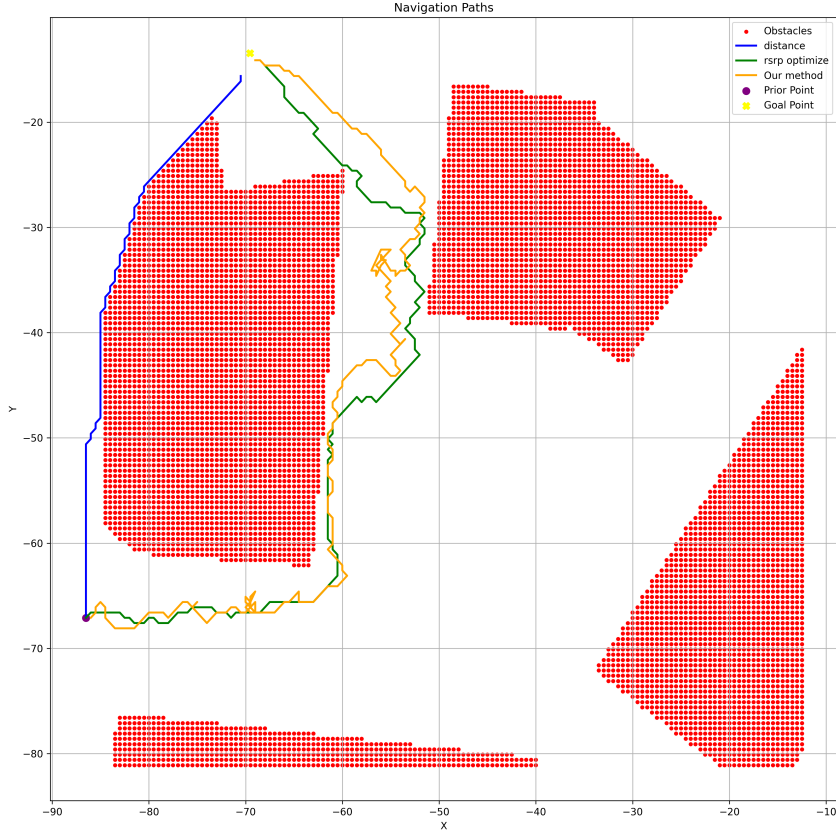Furthermore, by comparing the RSRP observations along the paths from both methods in

Figure 9: Route Map for Three Navigation Methods.

Figure17, we find that the ray-tracing simulation-based method repeatedly enters regions where the signal falls below the threshold. This suggests that the ray-tracing simulation erroneously predicts the signal when entering these regions, causing the robot to unexpectedly traverse areas with poor RSRP. In contrast, in our method the signal only dips below the threshold at two points.

Compared to the method that solely relies on ray-tracing simulation, our method incorporates GPR to capture the discrepancy between the observed and predicted RSRP values, which is then used to update $\mathcal{M}_{rsrp}$. The GPR thus plays a direct role in maintaining network connectivity in our method.
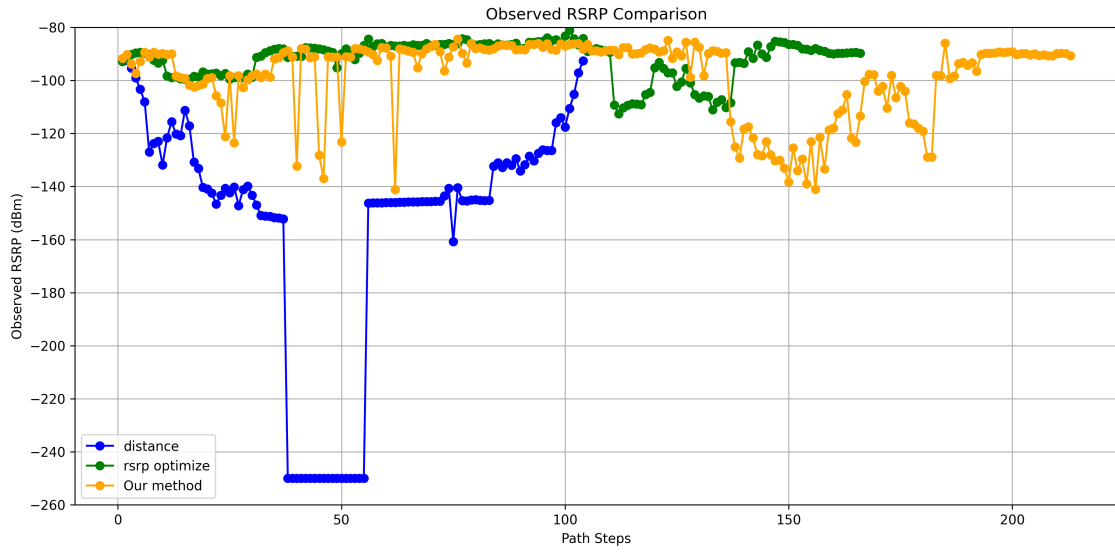
Figure 10: RSRP Distribution Along Routes for Three Navigation Methods.
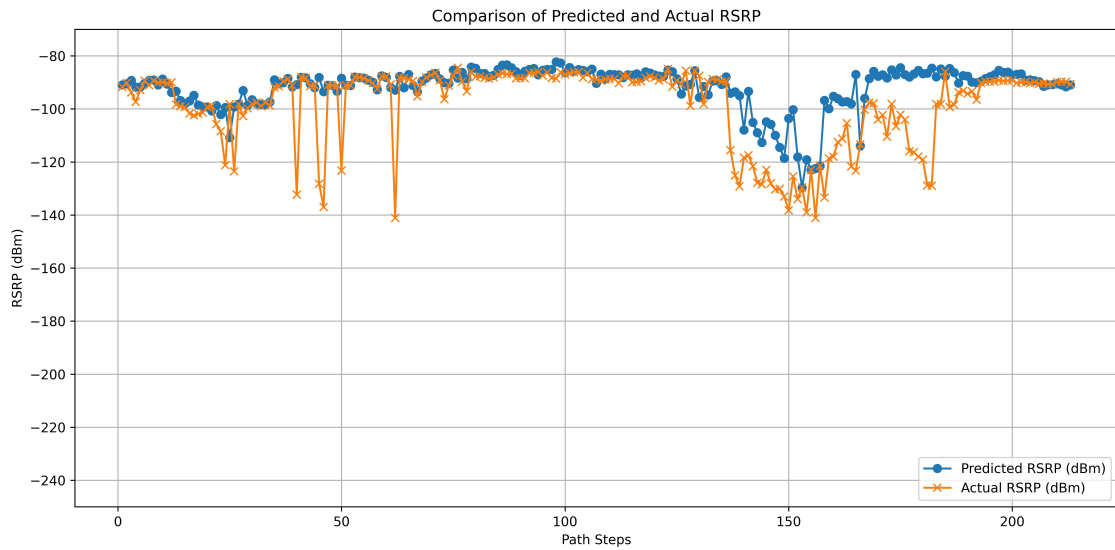
Figure 11: Predicted and Observed RSRP Values Along the Path by out method. Blue Dots: Predicted values, Yellow Dots: Observed values.
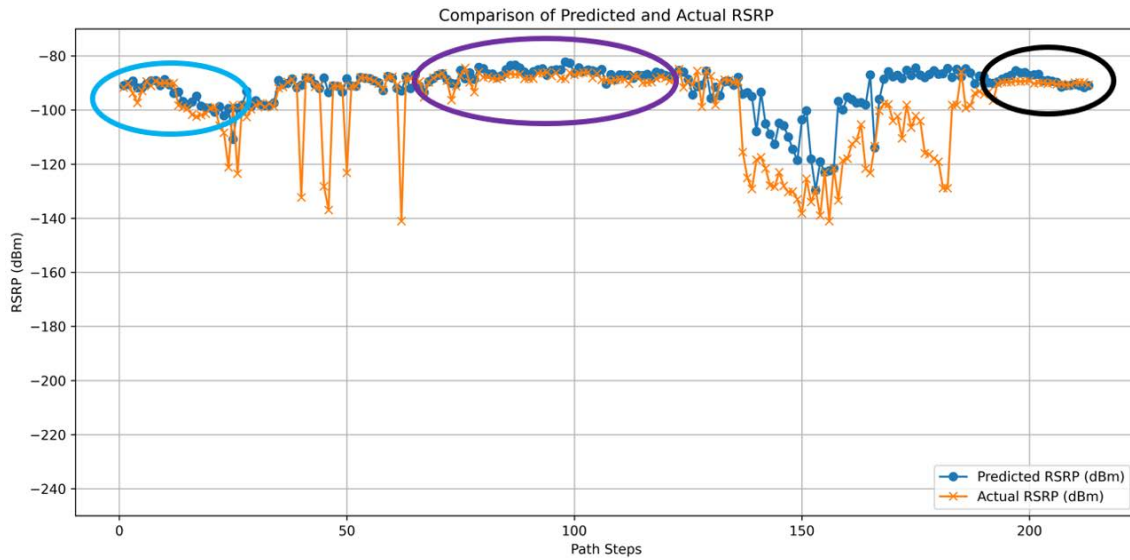
Figure 12: Path segments where the predicted and observed RSRP values are closely matched in our method,
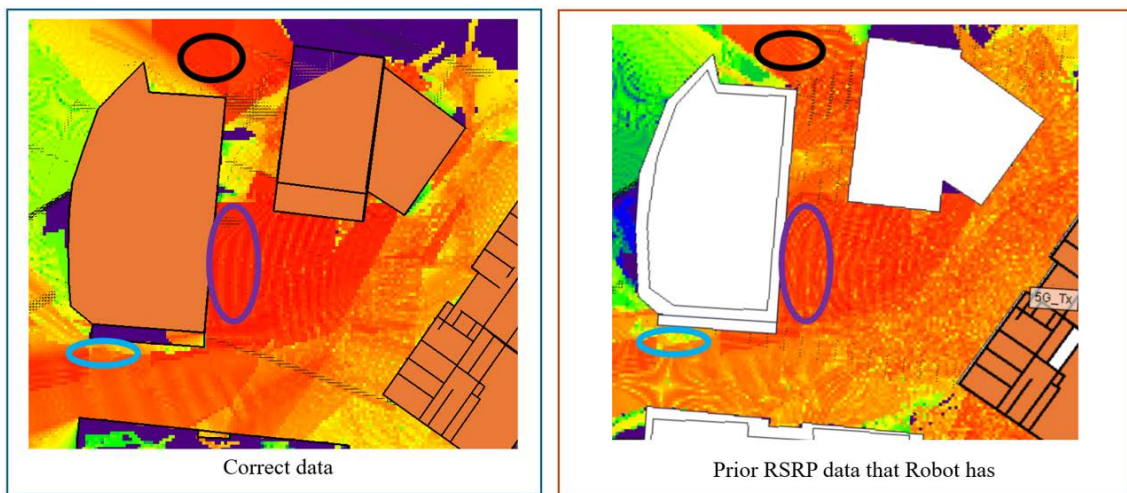
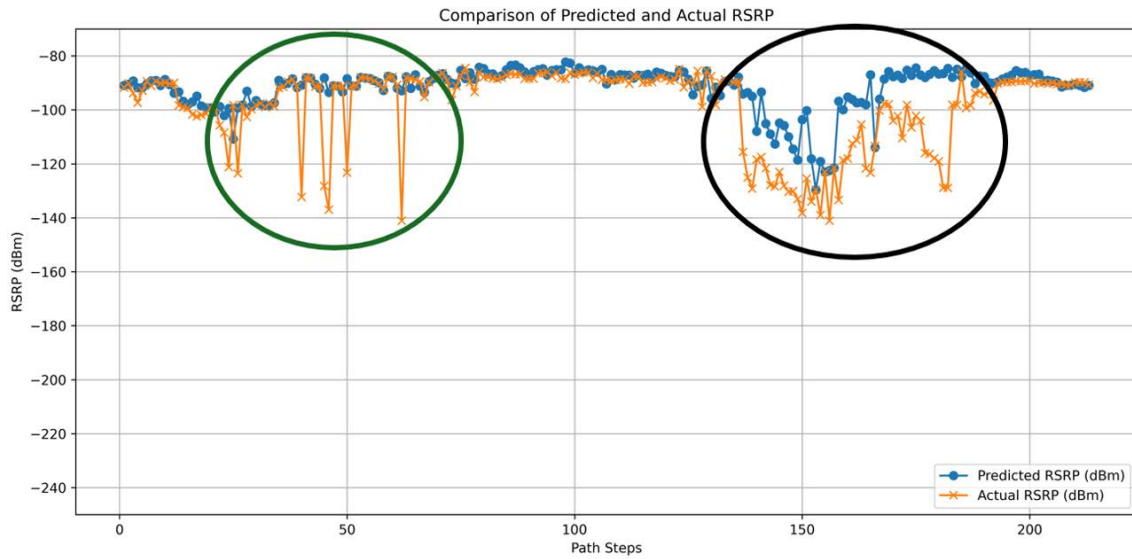Figure 13: Path segments in the corresponding regions matched by our method.

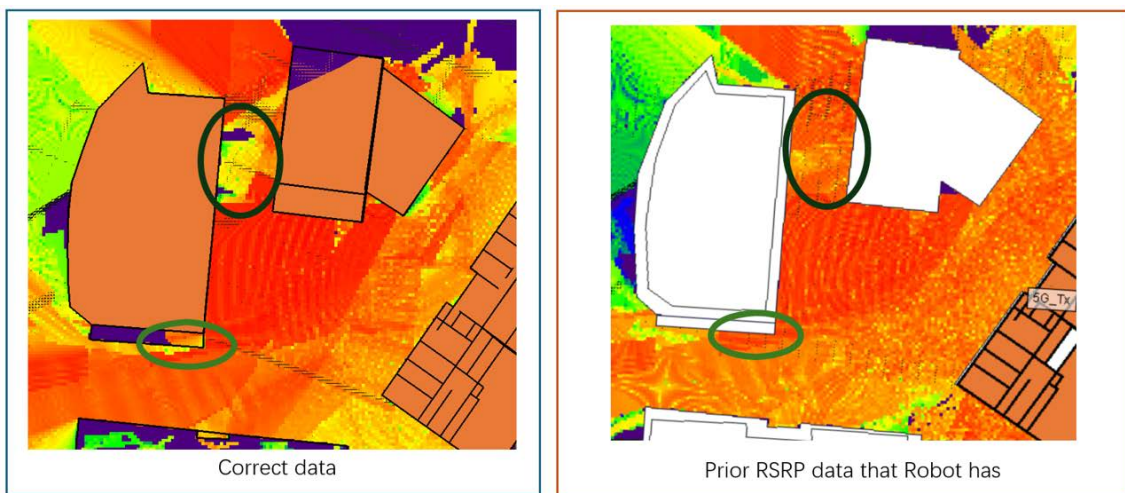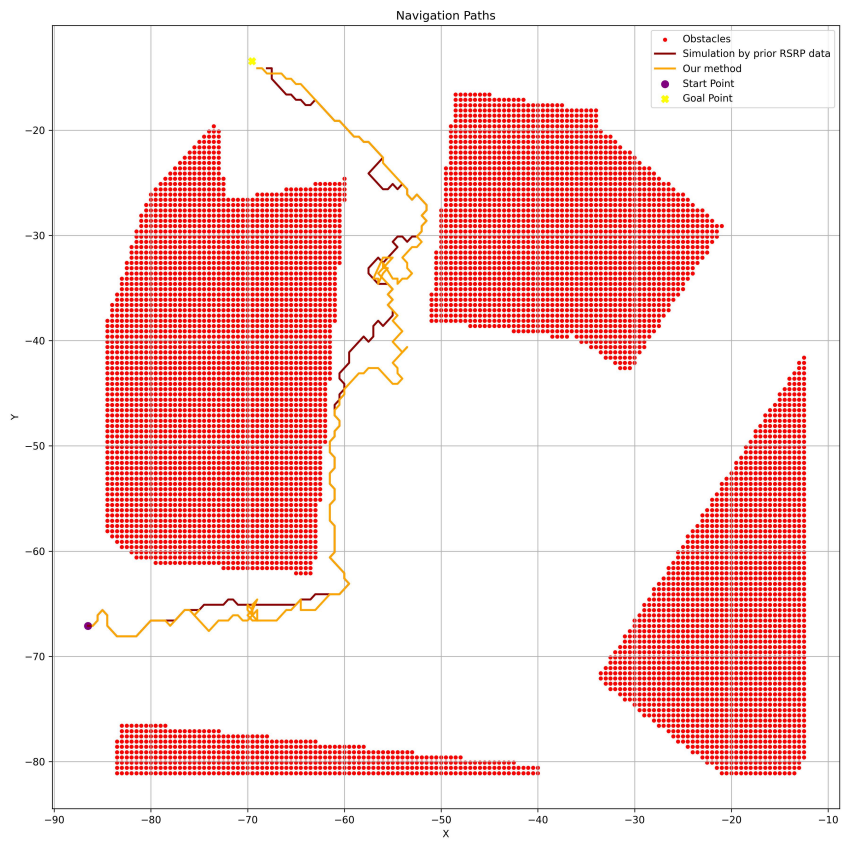Figure 14: Path segments where the predicted and observed RSRP values have large errors in our method,

Figure 15: Path segments in the corresponding regions matched by our method.

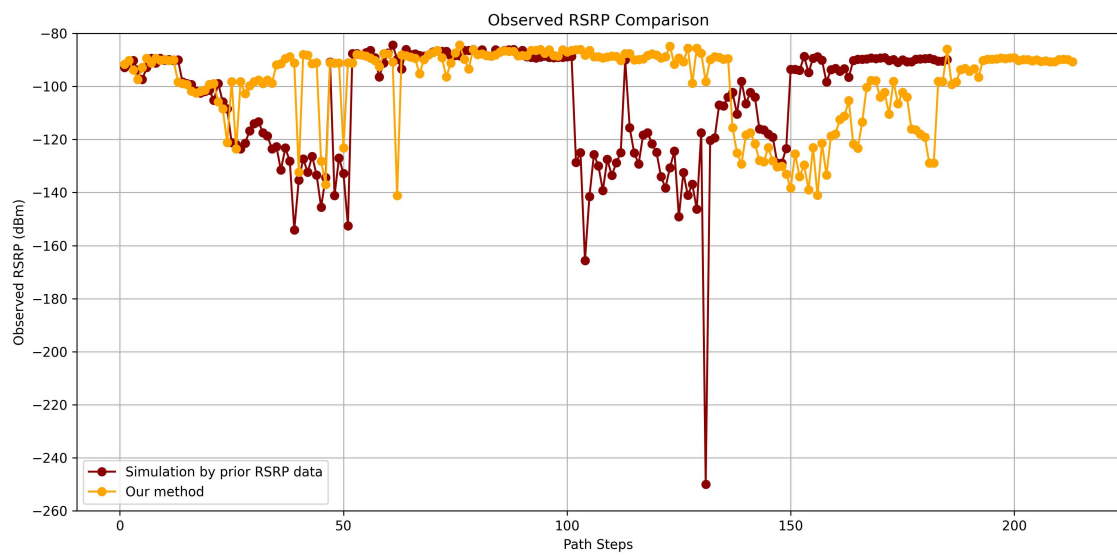Figure 16: Paths generated by our method and the method using only ray-tracing simulation,

Figure 17: RSRP observed along the paths generated by our method and the method using only ray-tracing simulation.

6 Conclusion

The widespread deployment of autonomous robots faces significant challenges in ensuring reliable communication for continuous network connectivity, particularly in urban environments where wireless signals are affected by multipath fading, obstacles, and environmental changes. Existing methods, while addressing robust communication, remain inadequate in dynamic environments due to their inability to account for rapid small-scale fading and their underutilization of robot sensing capabilities.

To address these limitations, this study proposes a navigation method that considers both Signal coefficient factor and Distance Cost within private 5G systems (Local 5G in Japan). The RSRP value is predicted utilizing ray-tracing simulation and GPR, while disconnection probability is quantified through a spatial Bayesian method and an empirical Nakagami-m distribution model. The effectiveness of the proposed method is evaluated through simulation experiments using ray-tracing simulation software *Wireless InSite*. The performance is assessed in terms of Distance Cost and RSRP levels along the route, with a penalty applied for weak signal regions. By integrating Signal coefficient factor navigation, the proposed method enables robots to efficiently reach their destinations while maintaining reliable network connection.

Acknowledgments

References

[1] L. Qiao, Y. Li, D. Chen, S. Serikawa, M. Guizani, and Z. Lv, "A survey on 5G/6G, AI, and robotics," *Computers and Electrical Engineering*, vol. 95, Art. ID 107372, Oct. 2021.

[2] D. Minoli and B. Occhiogrosso, "Practical aspects for the integration of 5G networks and IoT applications in smart cities environments," *Wireless Communications and Mobile Computing*, vol. 2019, no. 1, Art. ID 5710834, Aug. 2019.

[3] J. G. Andrews, S. Buzzi, W. Choi, *et al.*, "What will 5G be?" *IEEE Journal on selected areas in communications*, vol. 32, no. 6, pp. 1065–1082, Jun. 2014.

[4] M. Lindhé, K. H. Johansson, and A. Bicchi, "An experimental study of exploiting multipath fading for robot communications," *Proceedings of the 3rd International Conference on Robotics Science and Systems (RSS)*, pp. 289–296, Jun. 2008.

[5] S. Wan, Z. Gu, and Q. Ni, "Cognitive computing and wireless communications on the edge for healthcare service robots," *Computer Communications*, vol. 149, pp. 99–106, Jan. 2020.

[6] X. Zhou, W. Liang, I. Kevin, *et al.*, "Decentralized P2P federated learning for privacy-preserving and resilient mobile robotic systems," *IEEE Wireless Communications*, vol. 30, no. 2, pp. 82–89, Apr. 2023.

[7] B. Zhang, Y. Wu, X. Yi, and X. Yang, "Joint communication-motion planning in wireless-connected robotic networks: Overview and design guidelines," *arXiv preprint arXiv:1511.02299*, Nov. 2015.

[8] A. Muralidharan and Y. Mostofi, "Communication-aware robotics: Exploiting motion for communication," *Annual Review of Control, Robotics, and Autonomous Systems*, vol. 4, pp. 115–139, Jan. 2021.

[9] M. Sarhan, M. Hashim, A. Ismail, *et al.*, "A device-to-device (D2D) communication between mobile robots using wireless communication protocol in dynamic environments," in *Proceedings of AIP Conference*, vol. 2998, Mar. 2024.

[10] J. Yan, L. Zhang, X. Yang, C. Chen, and X. Guan, "Communication-aware motion planning of auv in obstacle-dense environment: A binocular vision-based deep learning method," *IEEE Transactions on Intelligent Transportation Systems*, vol. 24, no. 12, Jul. 2023.

[11] R. Parasuraman, B.-C. Min, and P. Ögren, "Rapid prediction of network quality in mobile robots," *Ad Hoc Networks*, vol. 138, Art.ID 103014, Jan. 2023.

[12] X. Wang, Y. Zhou, and J. Li, "Rcamp: A resilient communication-aware motion planner for mobile robots," *IEEE Transactions on Robotics*, vol. 33, no. 3, pp. 560–575, Dec. 2017.

[13] A. Pandey, S. Pandey, and D. Parhi, "Mobile robot navigation and obstacle avoidance techniques: A review," *International Robotics Automation Journal*, vol. 2, no. 3, Art. ID 00022, May. 2017.

[14] R. Parasuraman, T. Fabry, L. Molinari, *et al.*, "A multi-sensor RSS spatial sensing-based robust stochastic optimization algorithm for enhanced wireless tethering," *Sensors*, vol. 14, no. 12, pp. 23 970–24 003, Dec. 2014.

[15] T. S. Rappaport, *Wireless communications: principles and practice*. Cambridge University Press, Feb. 2024.

[16] Remcom Inc., *Wireless insite, version 3.1*, Computer software, 2021. [Online]. Available: `https://www.remcom.com/wireless-insite.html`.